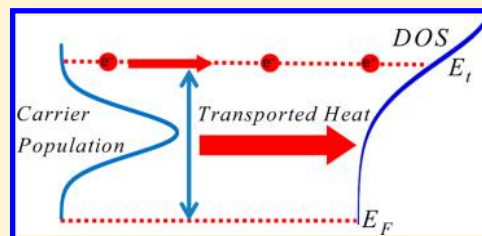# Thermoelectricity in Disordered Organic Semiconductors under the Premise of the Gaussian Disorder Model and Its Variants

Dan Mendels and Nir Tessler*

The Sarah and Moshe Zisapel Nanoelectronic Center, Electrical Engineering Department, Technion Israel Institute of Technology, Haifa 32000, Israel

**ABSTRACT:** Using Monte Carlo simulations, we investigate the thermo-electric properties of disordered organic semiconductors under the premise of the Gaussian disorder model and its variants. In doing so, we provide much needed additional dimensions for comparison between these theoretical frameworks and real systems beyond those based on extensively studied charge-transport properties and aim to provide a frame-of-reference for rising interest in these systems for thermoelectric-based applications. To illustrate the potential existing in the implementation of combined transport and thermoelectric investigation, we discuss strategies to experimentally deduce a



system's DOS shape and the temperature dependence of its transport energy (which can discern hopping transport from multiple trapping transport), infer whether a system's activation energy originates from inherent energetic disorder or a polaron activation energy (while deducing the given polaron activation energy), and discerning whether a system's energetic disorder is spatially correlated or accompanied by off-diagonal disorder.

**SECTION:** Energy Conversion and Storage; Energy and Charge Transport

Disordered organic semiconductor based electro-optic devices have in recent decades been primarily analyzed with a variety of phenomenological models,[1−10] prominent of which are those stemming from the Gaussian disorder model (GDM) put forward by Bassler and coauthors.[11] The latter's wide implementation has, in particular, attracted considerable attention in recent years, invoking efforts to devise analytic representations for these models[3,6,12−15] and implement them in practical device simulations.[16−20] Their validity and accuracy have been questioned, nevertheless, despite frequent agreement between experimental data and model outputs. This is due to the large number of free parameters that they possess, which facilitate such agreement, and their deficiency to consistently account for sets of experiments while keeping all model parameters constant.

Given these hindrances, in this Letter, we explore a path to promote deeper understanding and more credible and accurate representations of the transport process in organic semi-conductors through substantially reducing the arbitrariness accompanying experimental analysis of these systems. The path incorporates the implementation of thermoelectric experiments in conjunction with transport experiments through which a considerable increase of the constraints to which models utilized for experimental data analysis need to abide. Namely, by adding the Seebeck dimension, the analysis should be more credible. To initialize this undertaking, we quantitatively study the thermoelectric properties arising from the GDM and its variants. Additionally, in doing so, we aim also to address recent rising interest in the thermoelectric properties of organic semiconducting systems,[21−26] providing such studies with a simple and accurate theoretical frame-of-reference stemming from this set of models. To study thermoelectricity under the premise of the GDM and its variants, we utilize Monte Carlo simulations (MCS), which enable the attainment of quantita-tively more accurate and robust results than those previously obtained through analytic approximations.[27,28] Prospects for elaborate model−experiment comparisons based on combined thermoelectric and transport measurements aimed toward attaining deeper understanding and a more accurate representation of the charge-transport mechanism in these systems will also be discussed and be presented in the second part of this Letter.

In this study, the thermoelectric properties of the systems under investigation were probed via measuring their Peltier coefficient $\Pi$[29−31] in the employed MCS.

$$\Pi = \frac{1}{q\sigma_{tot}} \int_{-\infty}^{\infty} (E - E_F)\sigma(E) \, dE \qquad (1)$$

In eq 1, $\sigma(E)$ is the energy-dependent conductivity, $\sigma_{tot} = \int_{-\infty}^{\infty} \sigma(E) \, dE$ is the total conductivity, $E_F$ the quasi-chemical potential, and $q$ is the carrier charge. In compliance with most experimental studies that measure the Seebeck coefficient ($S$), we use the relation presented in eq 2[32] to present results in the form of the system's Seebeck coefficient

$$S = \frac{\Pi}{T} \qquad (2)$$

We recall that the Seebeck coefficient is defined or measured based on the relation shown in eq 3

$$S = \frac{\Delta V}{\Delta T} \tag{3}$$

where in eq 3, $\Delta V$ is the electrochemical drop within the system due to the applied temperature drop $\Delta T$ and $T$ in eq 2 is the system average temperature.

Simulations were implemented on a three-dimensional cubic lattice for which periodic boundary conditions were defined. Each site in the lattice, representing a localized carrier wave function, was assigned an energy drawn randomly from the system density of states (DOS), which for concreteness was taken to be a Gaussian function. We do not expect that the use of other typical DOS functions attributed to disordered organic semiconductors will principally alter the results and conclusions of this study.

$$g(E) = N_0 \frac{1}{\sqrt{2\pi\delta^2}} e^{-E^2/2\delta^2} \tag{4}$$

In eq 4, $\delta$ is the DOS standard deviation, and $N_0$ is the total state density.

Charge carrier propagation in the simulations occurred via stochastic hopping/charge-transfer events between lattice sites, where the occupancy of a single site by more than one carrier was prohibited due to the high energy associated with the Coulomb interaction between two closely placed carriers. For the sake of comparison between the thermoelectric properties of bare charge-transport and polaron transport, both Miller–Abrahams hopping[33] and Marcus[34] theory charge transfer were used. These are shown in eqs 5 and 6, respectively.

$$W_{ij} = \nu_0 \exp\left(-2\gamma r_{ij} - \frac{(E_j - E_i) + |E_j - E_i|}{2K_B T}\right) \tag{5}$$

$$W_{ij} = \frac{J_0^2}{\hbar} \sqrt{\left(\frac{\pi}{4E_a K_B T}\right)} \exp\left(-\frac{E_a}{K_B T}\right)$$
$$\times \exp\left(-2\gamma r_{ij} - \frac{(E_j - E_i)}{2K_B T} - \frac{(E_j - E_i)^2}{16K_B T E_a}\right) \tag{6}$$

Equations 5 and 6 express the hopping rates between site $i$ and site $j$, $E_i$ and $E_j$ represent the site energies, $r_{ij}$ is the effective distance between the sites, and $K_B$ is the Boltzmann's constant. The $\nu_0$ in eq 5 is the hopping attempt rate coefficient, and $E_a$ in eq 6 is the polaron activation energy. The transfer integral $J_0$ connecting sites $i$ and $j$, appearing in eq 6, was taken to be $J_0 = \exp(-2\gamma r_{ij})$, where $\gamma$, also appearing in eq 5, represents the carrier inverse localization length. For the sake of completeness, we note that alternative expressions to eqs 5 and 6, which have been imported from extraneous fields in physics, have been theoretically devised specifically for such systems and subsequent conductive, and thermoelectric properties resulting from them have been discussed in refs 31, 35, and 36. These frameworks are, nevertheless, not within the scope of this present study.

During a simulation run, every hopping event time and destination was determined by drawing a random dwell time via eq 7 for the origin site closest 125 neighboring sites and selecting the site associated with the shortest drawn dwell time.

$$\tau_{ij} = -\frac{1}{W_{ij}} \ln(x) \tag{7}$$

Here, $x$ is a number generated randomly within the interval [0,1]. In all simulations, the system total DOS was $N_0 = 10^{21}$ cm$^{-3}$, the average distance between nearest-neighboring sites being $a = 10^{-7}$ cm and the inverse localization length being $\gamma = 5 \times 10^7$ cm$^{-1}$. All simulations were run under low field conditions with $F = 10^3$ V/cm. More information regarding the dynamic MCS can be found in refs 11, 15, 37, and 38.

To expand the physical picture, we also included spatial correlations (correlated GDM) and off-diagonal disorder (off-diagonal GDM). Spatial correlations were introduced following ref 1, where initially all sites were assigned energy values $U_i$ drawn randomly from the DOS function and subsequently were replaced by the spatially averaged energy values calculated using eq 8

$$E_i = N^{1/2} \sum_j M(r_{ij}) U_j \tag{8}$$

where

$$M(r_{ij}) = \begin{cases} 1 & r_{ij} \le K \\ 0 & r_{ij} > K \end{cases} \tag{9}$$

In eqs 8 and 9 $N$ is the normalization factor set to yield the desired DOS standard deviation, and $K$ is the cutoff radius determining the number of sites over which averaging is performed.

Off-diagonal disorder, usually attributed to the variability of molecular orbital orientations and positions in realistic systems,[10,11,39] was introduced following ref 10. Variability of the transfer integrals corresponding to neighboring molecules was implemented by drawing the effective distance $r_{ij}$ between nearest-neighboring and next-nearest-neighboring sites randomly from the interval $[R_{ij} - \Gamma, R_{ij} + \Gamma]$, where $R_{ij}$ is the effective distance between sites prior to including the off-diagonal disorder and $\Gamma$ is the parameter defining the disorder magnitude. Unphysically high transfer integrals were prohibited, and a minimum cutoff effective distance of $r_{ij} = (1/2)a$ between sites was enforced.

Measurement of the Peltier coefficient (eq 1) in the simulations required measuring the system energy-dependent conductivity function $\sigma(E)$ and calculating the system's quasi-chemical potential via eq 10

$$n = \int_{-\infty}^{\infty} g(E) f(E, E_F)\, dE \tag{10}$$

where $n$ is the carrier density in the system and $f(E,E_F)$ is the Fermi–Dirac distribution function. Direct measurement of the energy-dependent conductivity was initially conducted by maintaining a histogram $D(E)$ of the distances hopped by carriers along and against the field bias as a function of energy. When a carrier hopped along (against) the field bias to a site with energy $E$, the distance that it hopped was added (reduced) to (from) $D(E)$. The current density $J(E)$, proportional to $D(E)$, and the conductivity $\sigma(E)$, proportional to $J(E)$ via Ohm's law, were subsequently calculated. This methodology was found to be consistent with that in ref 31 given that eq 5 was used to express the carriers' hopping rates and consistent to a good approximation provided that eq 6 was used (see eq 5 in ref 31).

Attaining sufficiently smooth results using the described methodology required, nevertheless, extremely long simulation times due to carrier adjacent site oscillations[15] and circular

3248

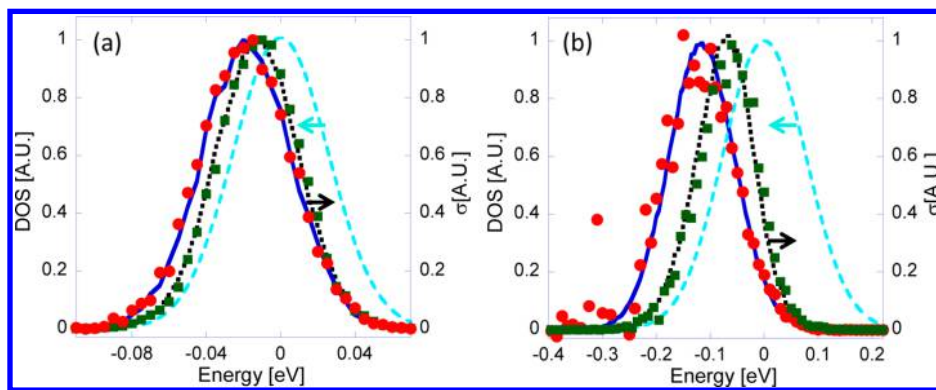dx.doi.org/10.1021/jz5016058 | J. Phys. Chem. Lett. 2014, 5, 3247–3253

**Figure 1.** Comparison between the direct (symbols) and approximate (solid and dotted lines) methods for measuring $\sigma(E)$ under the premise of the GDM (squares and dotted lines) and the correlated GDM (circles and solid lines) for which $K = 3$. Results in (a) were obtained from simulations run with a DOS standard deviation of $\delta = K_{B}T_0$ (DOS functions represented with dashed lines), and those in (b) are from simulations run with $\delta = 3K_{B}T_0$, where $T_0 = 298$ K. All data were obtained from simulations run at $T = 300$ K and with carrier density $n = 10^{17}$ cm$^{-3}$.
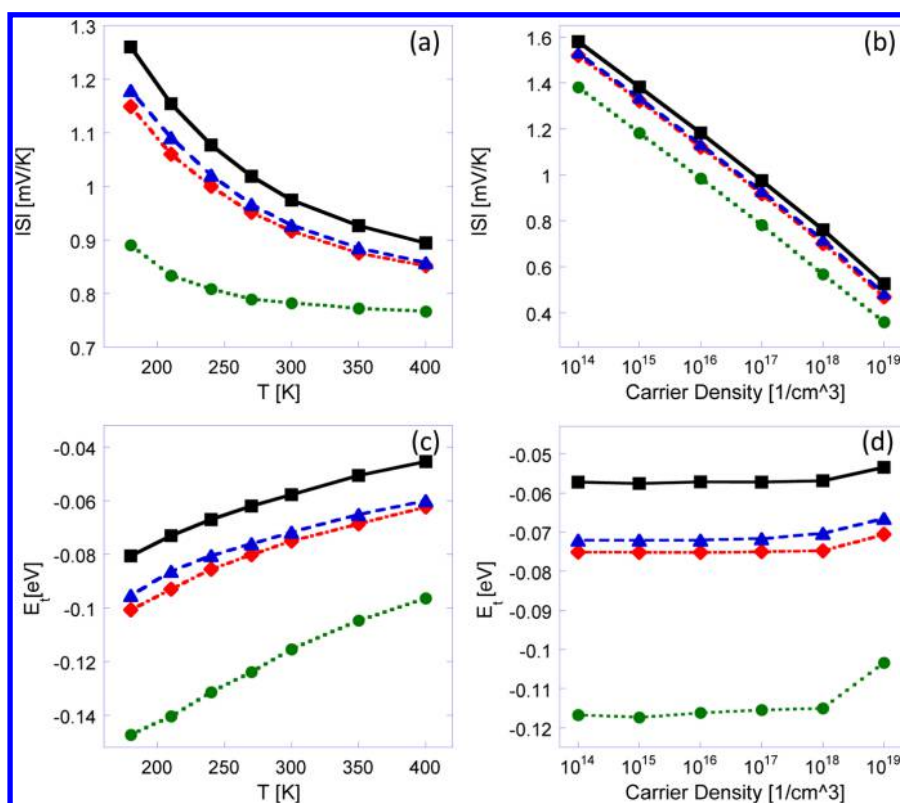


**Figure 2.** Seebeck coefficient values obtained from MCS (a) as a function of temperature with carier density $n = 10^{17}$ cm$^{-3}$ and (b) as a function of the carrier density at temperature $T = 300$ K. (c,d) Transport energy $E_t$ as a function of carrier density at temperature $T = 300$ K and as a function of temperature with carrier density $n = 10^{17}$ cm$^{-3}$, respectively. All results were obtained for a system with a Gaussian DOS with standard deviation of $\delta = 3K_{B}T_0$. In all subfigures, diamonds correspond to the GDM, circles to the correlated GDM, with $K = 3$, triangles to the GDM implemented under the premise of polaron transport with an activation energy $E_a = 0.15$ eV, and squares to the off-diagonal GDM, with $\Gamma = 0.7a$.

trajectories. Thus, to circumvent this hindrance, a considerably more efficient approximate method was devised. In it, only hopping events in which a carrier hopped into a lattice plane that it had *not* previously visited were registered in $D(E)$. (Note that events in which a carrier arrived to a lattice plane that it had previously visited, but did so *after* propagating through a periodic lattice boundary an odd number of times since its last visit, were accounted for in $D(E)$.)

A comparison between the normalized energy-dependent conductivity functions $\sigma(E)$ attained by the two methods described above is presented in Figure 1. This figure shows the

measured conductivity as a function of energy, $\sigma(E)$, taking the center of the DOS as $E = 0$. Figure 1a presents results for DOS standard deviation $\delta = 1K_{B}T_0$, and Figure 1b shows those for $\delta = 3K_{B}T_0$, where $T_0 = 298$ K and the assumed carrier density was $10^{17}$ cm$^{-3}$. Note that while we indicate absolute charge densities in the simulations, it is the fraction of the total DOS $(N_0)$ that is of physical importance. The symbols represent results obtained through the direct method, and the lines are the results of the approximated, and fast, method. The square symbols and dotted lines were calculated using the GDM picture and, round symbols and full lines are the result of
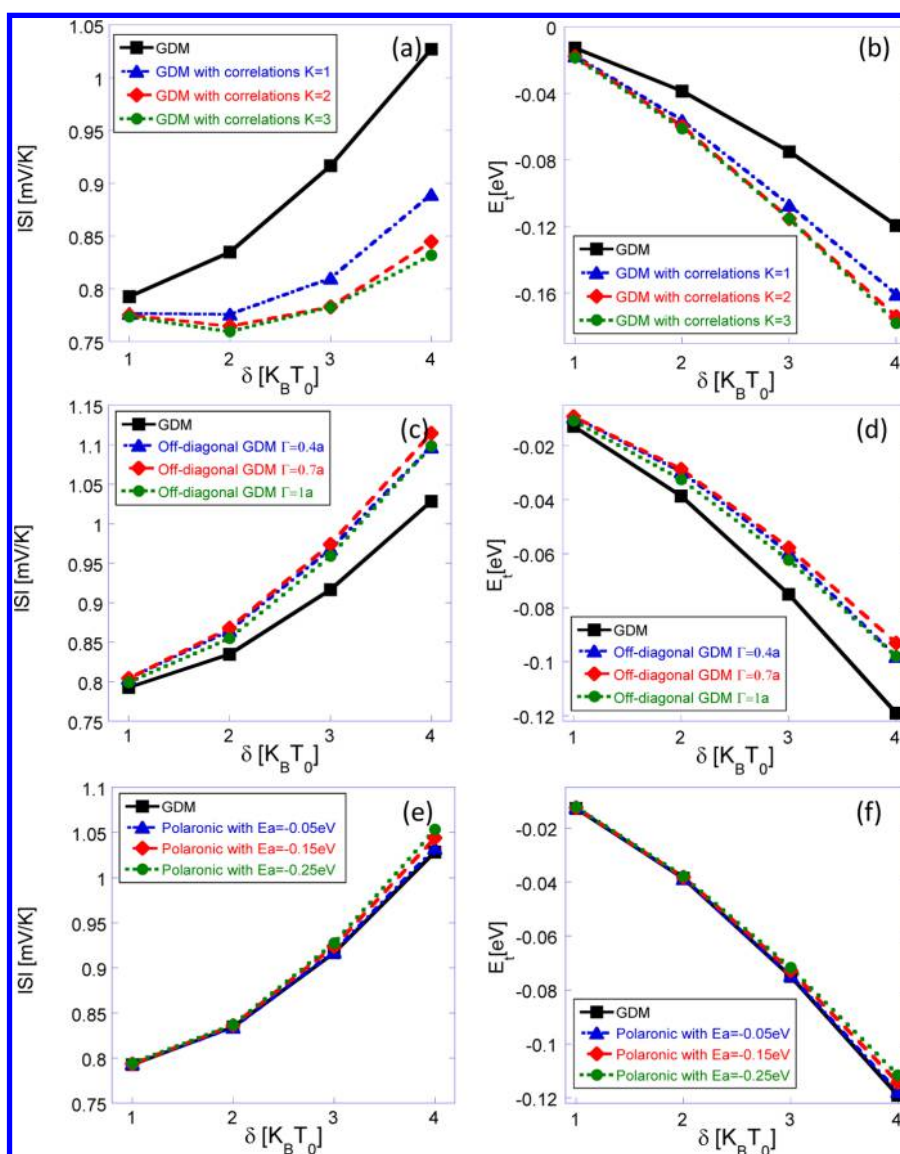
**Figure 3.** (a,c,e) Seebeck coefficient and (b,d,f) transport energy as a function of $\delta$ for different physical scenarios. (a,b) Correlated GDM, (c,d) off-diagonal GDM, and (e,f) the GDM implemented under the premise of polaron transport. All corresponding model parameter values are presented in subfigure legends.

the correlated GDM model. Good agreement between the outputs of the two methods can be observed. Using the data in Figure 1 and eq 1, we calculated the Peltier coefficients resulting from the direct and approximated method. We found a deviation of only ~0.3% for $\delta = 1K_BT_0$ and ~2% for $\delta = 3K_BT_0$ between the two methods. In the context of the present study, these differences are negligible.

For the rest of the paper, we present results that were obtained by utilizing the approximate method only to measure $\sigma(E)$. The thermoelectric properties of the GDM were calculated with the aid of eqs 1, 2, and 10 as a function of temperature, carrier density, and disorder parameter $\delta$. Similarly, the thermoelectric properties as a function of the aforementioned variables were subsequently calculated under the premise of the GDM variants in which either spatial correlations in the system's energetic landscape were incorporated, off-diagonal disorder was included, or the Miller–Abrahams hopping expression, eq 5, was replaced with that of Marcus theory, eq 6. For convenience sake, results

are presented in the form of the absolute values of the computed Seebeck coefficients and are referred to in the text for conciseness as the "Seebeck coefficient values" rather than the "absolute values of the Seebeck coefficients".

Results in Figure 2 were calculated for disorder parameter $\delta = 3K_BT_0$. Figure 2a shows the Seebeck coefficient measured as a function of temperature (for $n = 10^{17}$ cm$^{-3}$), and Figure 2b shows it as a function of carrier density (for $T = 300$ K). The various lines correspond to the different models used. These are the GDM (diamonds), the correlated GDM (circles), the off-diagonal disorder GDM (squares), and the GDM under the premise of polaron transport (triangles). To facilitate the physical understanding, we show in Figure 2c and d the corresponding transport energy values deduced using $E_t = \left( \int_{-\infty}^{\infty} \sigma(E)E \, dE / \int_{-\infty}^{\infty} \sigma(E) \, dE \right)$.

As Figure 2 shows, the functional form of the Seebeck coefficient is similar for all of the physical scenarios tested and cannot be used to experimentally differentiate between them. In fact, the Seebeck coefficient dependence on carrier density and

temperature exhibited in Figure 2 corresponds qualitatively to experimental results found in the literature.[40−42] Figure 2 teaches us two additional important issues. First, unlike the mobility[43] or the carrier heating phenomena,[44] the Seebeck coefficient is practically not affected by the existence of a polaron binding energy[29] as the differences found are within the 2% error of our method. Second, spatial correlation or off-diagonal disorder would decrease and increase the Seebeck coefficient, respectively. These differences can be understood with the aid of Figure 2c and d. Incorporating spatial correlations within the system energetic landscape results in the lowering of the transport energy and decrease of the Seebeck coefficient. Alternatively, the inclusion of off-diagonal disorder in the system results in the rising of the transport energy and increase of the Seebeck coefficient. Regarding the GDM itself, transport energy values obtained in this study are lower by 50−100 meV than transport energy values found in refs 13 and 14 but do coincide with transport energy values calculated in ref 15. (We note that as pointed out in ref 45, the discrepancy between the aforementioned methods results from a difference in the quantity that is being calculated. Namely, while here and in ref 15 it is the energy through which most carrier propagation occurs, in refs 13 and 14, it is the effective energy affiliated with the rate-determining step of the transport process.[45])

As the degree of disorder varies between materials, we look into the effect of the disorder parameter, $\delta$. The Seebeck coefficient and transport energy dependence on the disorder parameter $\delta$ under the premise of the different model variants for a range of parameter values are presented in Figure 3. The data were obtained from simulations run at $T = 300$ K and carrier density of $n = 10^{17}$ cm$^{-3}$. In Figure 3a and b, the lowering of the transport level and decrease of the Seebeck coefficient due to the incorporation of spatial correlations within the system energetic landscape can be seen to be augmented as $\delta$ increases. The predominant effect seems to follow the actual incorporation of correlations ($K = 1$), while a further increase of the spatial correlation parameter leads to a somewhat weaker effect.

The rising of the transport energy and increase of the Seebeck coefficient (seen in Figure 3c and d) due to the inclusion of off-diagonal disorder in the GDM can be seen to also be augmented as $\delta$ increases. Concomitantly, the incorporation of moderate off-diagonal disorder ($\Gamma = 0.4a$) seems sufficient to give rise to the most noticeable effect, while further increase of $\Gamma$ leads to slighter attenuations in the computed values. The rising of the transport energy due to the inclusion of off-diagonal disorder can be attributed to the reduction of approximately half of the distances between nearest-neighboring sites in the system, thereby rendering higher-energy sites as more probable hopping destinations. Conversely, spatial correlations within the system energetic landscape increase the probability for carriers to locate hopping destinations nearer in energy to their origin site energy, thereby leading to an overall decrease of the energies that carriers attain when propagating through the system.

Figure 3e and f corresponds to Figure 2 as well showing that Seebeck coefficient and transport energy values obtained from simulations run with different polaron activation energies are notably similar to those obtained in simulations of bare charge carrier transport (eq 5).

Results presented in this Letter manifest the information contained in the thermoelectric properties of disordered organic semiconductors regarding charge transport in these systems. It can, thus, be deduced that conducting combined thermoelectric and transport experiments would lead to more robust, accurate, and transparent representations of the charge-transport process in these systems. To be concrete, we bring below a few examples of how such a combination can be beneficially used in experiments.

As a first example, extracting the DOS function within an organic field effect transistor channel can be done using charge carrier density-dependent measurements of the Seebeck coefficient. As seen in Figure 2, the transport energy depends very weakly on the carrier density up to very high densities; hence, by measuring the Seebeck coefficient as a function of gate voltage $S(V_G)$, one can deduce the dependence of the system quasi-chemical potential on the applied gate voltage $E_F(V_G)$. Concomitantly, the system carrier density dependence on the applied gate voltage $n(V_G)$ can be obtained using a methodology such as that utilized in refs 46 and 47. Consequently, the relation between the carrier density and the system quasi-chemical potential $n(E_F)$ can be deduced and from it, via eq 10, the system DOS $g(E)$. Moreover, because the numerical method to calculate the Seebeck coefficient presented here is fast, it is possible to run it using a varying DOS function to obtain best fits to real DOS functions, that is, beyond Gaussian only.

Reports on high-mobility organic materials have resurfaced the question whether the transport in such materials should be described as hopping transport or would be better described using the multiple trapping scenario in the presence of extended band-like states. On the basis of the results shown in Figure 2, we suggest addressing this question using temperature-dependent measurements. While within hopping transport the transport energy is noticeably temperature-dependent (Figure 2d), the mobility edge in multitrapping transport is temperature-independent given that the band gap temperature dependence[48] is factored out. Thus, having established the shape of the DOS either through the above method or other methods,[9,46] it is possible to deduce $E_F(T)$ for a given charge density using a methodology similar to that presented in ref 49. With this information, the temperature dependence of the transport energy can be deduced from $E_t(T) = qT \cdot S(T) + E_F(T)$, and from it, the nature of the states that are located in it can be deduced.

An additional prospect arising from the presented results is the ability to discern the extent to which a system's activation energy is associated with energetic disorder or a polaronic activation energy. The near equality of the transport energy values corresponding to bare charge transport and polaron transport reveals that through measuring a system's transport *and* thermoelectric properties, its polaronic activation energy can be deduced. This is due to the polaronic activation energy finding manifestation in the mobility of the system (every carrier step in the system is slowed on average by a factor proportional to $\exp(-E_a/K_BT)$) while finding only very minute, if at all, manifestation in the system's Seebeck coefficient, as seen in Figures 2 and 3.

Assuming that transport can indeed be described using the GDM and its variants, another immediate implication is the possibility to examine the consistency of the incorporation of spatial correlations in the system's energetic landscape or the inclusion of off-diagonal disorder with thermoelectric experimental data. The above are known to bear signatures on the system's mobility field dependence[1,10,11] and, where observed,

can, using the framework presented here, be cross correlated with system Seebeck coefficient values. For example, the attribution of the Pool−Frenkel behavior over a wide range of fields present in many disordered organic systems to spatial correlations[1] can be reinspected and subsequently strengthened or refuted. This may be done by extracting the GDM parameters yielding the best fits to a system's experimental mobility field dependence and using the framework presented here to compare Seebeck coefficient values obtained for the model with those measured experimentally.

To conclude, in this Letter, we have investigated the thermoelectric properties of disordered organic semiconductors under the premise of the GDM and its variants. In doing so, we have aimed to address recent raising interest in the disordered organic semiconductors' potential for thermoelectric applications and provide new dimensions to quantitatively compare between the GDM framework and its variants with real systems. Such comparisons conducted along with standard transport measurements, as discussed above, bear the potential to elucidate qualitative aspects regarding the transport process as well as advance the capabilities to model it more accurately and credibly.

## ■ AUTHOR INFORMATION

**Corresponding Author**

*E-mail: nir@ee.technion.ac.il. Phone: +972 4 8294719. Fax: +972 4 8294719. Website: www.ee.technion.ac.il/nir.

**Notes**

The authors declare no competing financial interest.

## ■ REFERENCES

(1) Gartstein, Yu.N.; Conwell, E. M. High-Field Hopping Mobility in Molecular Systems with Spatially Correlated Energetic Disorder. *Chem. Phys. Lett.* **1995**, *245*, 351−358.

(2) Novikov, S.; Dunlap, D.; Kenkre, V.; Parris, P.; Vannikov, A. Essential Role of Correlations in Governing Charge Transport in Disordered Organic Materials. *Phys. Rev. Lett.* **1998**, *81*, 4472−4475.

(3) Tessler, N.; Preezant, Y.; Rappaport, N.; Roichman, Y. Charge Transport in Disordered Organic Materials and Its Relevance to Thin-Film Devices: A Tutorial Review. *Adv. Mater.* **2009**, *21*, 2741−2761.

(4) Gonzalez-Vazquez, J. P.; Anta, J. A.; Bisquert, J. Random Walk Numerical Simulation for Hopping Transport at Finite Carrier Concentrations: Diffusion Coefficient and Transport Energy Concept. *Phys. Chem. Chem. Phys.* **2009**, *11*, 10359−10367.

(5) Kreouzis, T.; Poplavskyy, D.; Tuladhar, S.; Campoy-Quiles, M.; Nelson, J.; Campbell, A.; Bradley, D. Temperature and Field Dependence of Hole Mobility in Poly(9,9-dioctylfluorene). *Phys. Rev. B* **2006**, *73*, 235201.

(6) Vissenberg, M. C. J. M.; Matters, M. Theory of the Field-Effect Mobility in Amorphous Organic Transistors. *Phys. Rev. B* **1998**, *57*, 964−967.

(7) Bassler, H.; Kohler, A. Charge Transport in Organic Semiconductors. *Top. Curr. Chem.* **2012**, *312*, 1−65.

(8) Parris, P.; Kenkre, V.; Dunlap, D. Nature of Charge Carriers in Disordered Molecular Solids: Are Polarons Compatible with Observations? *Phys. Rev. Lett.* **2001**, *87*, 126601.

(9) Oelerich, J. O.; Huemmer, D.; Baranovskii, S. D. How to Find Out the Density of States in Disordered Organic Semiconductors. *Phys. Rev. Lett.* **2012**, *108*, 226403.

(10) Gartstein, Y. N.; Conwell, E. M. High-Field Hopping Mobility in Disordered Molecular Solids: A Monte Carlo Study of Off-Diagonal Disorder Effects. *J. Chem. Phys.* **1994**, *100*, 9175.

(11) Bassler, H. Charge Transport in Disordered Organic Photoconductors. *Phys. Status Solidi B* **1993**, 15.

(12) Fishchuk, I. I.; Arkhipov, V. I.; Kadashchuk, A.; Heremans, P.; Bässler, H. Analytic Model of Hopping Mobility at Large Charge Carrier Concentrations in Disordered Organic Semiconductors: Polarons versus Bare Charge Carriers. *Phys. Rev. B* **2007**, *76*, 045210.

(13) Arkhipov, V. I.; Emelianova, E. V.; Adriaenssens, G. J. Effective Transport Energy versus the Energy of Most Probable Jumps in Disordered Hopping Systems. *Phys. Rev. B* **2001**, *64*, 125125.

(14) Baranovskii, S. D.; Faber, T.; Hensel, F.; Thomas, P. The Applicability of the Transport-Energy Concept to Various Disordered Materials. *J. Phys.: Condens. Matter* **1997**, *9*, 2699.

(15) Mendels, D.; Tessler, N. The Topology of Hopping in the Energy Domain of Systems with Rapidly Decaying Density of States. *J. Phys. Chem. C* **2013**, *117*, 24740−24745.

(16) Mesta, M.; Carvelli, M.; De Vries, R. J.; Van Eersel, H.; Van der Holst, J. J. M.; Schober, M.; Furno, M.; Lüssem, B.; Leo, K.; Loebl, P.; et al. Molecular-Scale Simulation of Electroluminescence in a Multilayer White Organic Light-Emitting Diode. *Nat. Mater.* **2013**, *12*, 652−658.

(17) Van der Holst, J. J. M.; Van Oost, F. W. a.; Coehoorn, R.; Bobbert, P. a. Monte Carlo Study of Charge Transport in Organic Sandwich-Type Single-Carrier Devices: Effects of Coulomb Interactions. *Phys. Rev. B* **2011**, *83*, 085206.

(18) Roichman, Y.; Preezant, Y.; Tessler, N. Analysis and Modeling of Organic Devices. *Phys. Status Solidi A* **2004**, *201*, 7514−7520.

(19) Groves, C.; Marsh, R. a; Greenham, N. C. Monte Carlo Modeling of Geminate Recombination in Polymer−Polymer Photovoltaic Devices. *J. Chem. Phys.* **2008**, *129*, 114903.

(20) Deibel, C.; Dyakonov, V. Polymer−Fullerene Bulk Heterojunction Solar Cells. *Rep. Prog. Phys.* **2010**, *73*, 096401.

(21) Kim, G.-H.; Shao, L.; Zhang, K.; Pipe, K. P. Engineered Doping of Organic Semiconductors for Enhanced Thermoelectric Efficiency. *Nat. Mater.* **2013**, *12*, 719−723.

(22) Zhang, Q.; Sun, Y.; Xu, W.; Zhu, D. Organic Thermoelectric Materials: Emerging Green Energy Materials Converting Heat to Electricity Directly and Efficiently. *Adv. Mater.* **2014**, DOI: 10.1002/adma.201305371.

(23) Bubnova, O.; Khan, Z. U.; Malti, A.; Braun, S.; Fahlman, M.; Berggren, M.; Crispin, X. Optimization of the Thermoelectric Figure of Merit in the Conducting Polymer Poly(3,4-ethylenedioxythiophene). *Nat. Mater.* **2011**, *10*, 429−433.

(24) Von Mühlenen, A.; Errien, N.; Schaer, M.; Bussac, M.-N.; Zuppiroli, L. Thermopower Measurements on Pentacene Transistors. *Phys. Rev. B* **2007**, *75*, 115338.

(25) Germs, W. C.; Guo, K.; Janssen, R. a. J.; Kemerink, M. Unusual Thermoelectric Behavior Indicating a Hopping to Bandlike Transport Transition in Pentacene. *Phys. Rev. Lett.* **2012**, *109*, 016601.

(26) Harada, K.; Sumino, M.; Adachi, C.; Tanaka, S.; Miyazaki, K. Improved Thermoelectric Performance of Organic Thin-Film Elements Utilizing a Bilayer Structure of Pentacene and 2,3,5,6-Tetrafluoro-7,7,8,8-tetracyanoquinodimethane (F$_4$-TCNQ). *Appl. Phys. Lett.* **2010**, *96*, 253304.

(27) Schmechel, R. Hopping Transport in Doped Organic Semiconductors: A Theoretical Approach and Its Application to P-Doped Zinc-phthalocyanine. *J. Appl. Phys.* **2003**, *93*, 4653.

(28) Kim, G.; Pipe, K. P. Thermoelectric Model to Characterize Carrier Transport in Organic Semiconductors. *Phys. Rev. B* **2012**, *86*, 085208.

(29) Mott, N. F. *Electronic Processes in Non-crystalline Materials*; Clarendon Press: Oxford, U.K., 1979.

(30) Fritzsche, H. A General Expression for the Thermoelectric Power. *Solid State Commun.* **1971**, *9*, 1813−1815.

(31) Emin, D. Thermoelectric Power Due to Electronic Hopping Motion. *Phys. Rev. Lett.* **1975**, *35*, 882.

(32) Onsager, L. Irreversible Processes. *Phys. Rev.* **1931**, *37*, 237−241.

(33) Miller, A.; Abrahams, E. Impurity Conduction at Low Concentrations. *Phys. Rev.* **1960**, *120*, 745.

(34) Marcus, R. A. Chemical and Electrochemical Electron-Transfer Theory. *Annu. Rev. Phys. Chem.* **1964**, *15*, 155−196.

3252

dx.doi.org/10.1021/jz5016058 | *J. Phys. Chem. Lett.* 2014, 5, 3247−3253

(35) Gorham-Bergeron, E.; Emin, D. Phonon-Assisted Hopping Due to Interaction with Both Acoustical and Optical Phonons. *Phys. Rev. B* **1977**, *15*, 3667.

(36) Emin, D. Enhanced Seebeck Coefficient from Carrier-Induced Vibrational Softening. *Phys. Rev. B* **1999**, *59*, 6205−6210.

(37) Watkins, P. K.; Walker, A. B.; Verschoor, G. L. B. Dynamical Monte Carlo Modelling of Organic Solar Cells: The Dependence of Internal Quantum Efficiency on Morphology. *Nano Lett.* **2005**, *5*, 1814−1818.

(38) Mendels, D.; Tessler, N. Drift and Diffusion in Disordered Organic Semiconductors: The Role of Charge Density and Charge Energy Transport. *J. Phys. Chem. C* **2013**, *117*, 3287−3293.

(39) Brédas, J. L.; Calbert, J. P.; Da Silva Filho, D. a; Cornil, J. Organic Semiconductors: A Theoretical Characterization of the Basic Parameters Governing Charge Transport. *Proc. Natl. Acad. Sci. U.S.A.* **2002**, *99*, 5804−5809.

(40) Maennig, B.; Pfeiffer, M.; Nollau, A.; Zhou, X.; Leo, K.; Simon, P. Controlled P-Type Doping of Polycrystalline and Amorphous Organic Layers: Self-Consistent Description of Conductivity and Field-Effect Mobility by a Microscopic Percolation Model. *Phys. Rev. B* **2001**, *64*, 195208.

(41) Xuan, Y.; Liu, X.; Desbief, S.; Leclère, P.; Fahlman, M.; Lazzaroni, R.; Berggren, M.; Cornil, J.; Emin, D.; Crispin, X. Thermoelectric Properties of Conducting Polymers: The Case of Poly(3-hexylthiophene). *Phys. Rev. B* **2010**, *82*, 115454.

(42) Nollau, A.; Pfeiffer, M.; Fritz, T.; Leo, K. Controlled *n*-Type Doping of a Molecular Organic Semiconductor: Naphthalenetetra-carboxylic Dianhydride (NTCDA) Doped with Bis(Ethylenedithio)-tetrathiafulvalene (BEDT-TTF). *J. Appl. Phys.* **2000**, *87*, 4340−4343.

(43) Arkhipov, V. I.; Heremans, P.; Emelianova, E. V.; Adriaenssens, G. J.; Bässler, H. Equilibrium Trap-Controlled and Hopping Transport of Polarons in Disordered Materials. *Chem. Phys.* **2003**, *288*, 51−55.

(44) Preezant, Y.; Tessler, N. Carrier Heating in Disordered Organic Semiconductors. *Phys. Rev. B* **2006**, *74*, 235202.

(45) Oelerich, J. O.; Jansson, F.; Nenashev, a. V.; Gebhard, F.; Baranovskii, S. D. Energy Position of the Transport Path in Disordered Organic Semiconductors. *J. Phys.: Condens. Matter* **2014**, *26*, 255801.

(46) Tal, O.; Rosenwaks, Y.; Preezant, Y.; Tessler, N.; Chan, C.; Kahn, A. Direct Determination of the Hole Density of States in Undoped and Doped Amorphous Organic Films with High Lateral Resolution. *Phys. Rev. Lett.* **2005**, *95*, 256405.

(47) Tal, O.; Epstein, I.; Snir, O.; Roichman, Y.; Ganot, Y.; Chan, C.; Kahn, A.; Tessler, N.; Rosenwaks, Y. Measurements of the Einstein Relation in Doped and Undoped Molecular Thin Films. *Phys. Rev. B* **2008**, *77*, 201201.

(48) Tessler, N.; Harrison, N. T.; Thomas, D. S.; Friend, R. H. Current Heating in Polymer Light Emitting Diodes. *Appl. Phys. Lett.* **1998**, *73*, 732.

(49) Mehraeen, S.; Coropceanu, V.; Brédas, J.-L. Role of Band States and Trap States in the Electrical Properties of Organic Semi-conductors: Hopping versus Mobility Edge Model. *Phys. Rev. B* **2013**, *87*, 195209.

## ■ NOTE ADDED AFTER ASAP PUBLICATION

This paper was published ASAP on September 9, 2014. Figure 3 was updated. The revised paper was reposted on September 10, 2014.